2012

A GGA plus U approach to effective electronic correlations in thiolate-ligated iron-oxo (IV) porphyrin

Justin Elenewski
Virginia Commonwealth University

John C. Hackett
Virginia Commonwealth University, jchackett@vcu.edu

Elenewski, J. E., and Hackett, J. C. A GGA plus U approach to effective electronic correlations in thiolate-ligated iron-oxo (IV) porphyrin. The Journal of Chemical Physics, 137, 124311 (2012). Copyright © 2012 American Institute of Physics.

A GGA+*U* approach to effective electronic correlations in thiolate-ligated iron-oxo (IV) porphyrin

Justin E. Elenewski and John C Hackett[a)]
Institute for Structural Biology and Drug Discovery and Department of Medicinal Chemistry, School of Pharmacy, Virginia Commonwealth University, 800 East Leigh Street, Richmond, Virginia 23219, USA

(Received 10 July 2012; accepted 9 September 2012; published online 28 September 2012)

High-valent oxo-metal complexes exhibit correlated electronic behavior on dense, low-lying electronic state manifolds, presenting challenging systems for electronic structure methods. Among these species, the iron-oxo (IV) porphyrin denoted Compound I occupies a privileged position, serving a broad spectrum of catalytic roles. The most reactive members of this family bear a thiolate axial ligand, exhibiting high activity toward molecular oxygen activation and substrate oxidation. The default approach to such systems has entailed the use of hybrid density functionals or multi-configurational/multireference methods to treat electronic correlation. An alternative approach is presented based on the GGA+*U* approximation to density functional theory, in which a generalized gradient approximation (GGA) functional is supplemented with a localization correction to treat on-site correlation as inspired by the Hubbard model. The electronic structure of thiolate-ligated iron-oxo (IV) porphyrin and corresponding Coulomb repulsion *U* are determined both empirically and self-consistently, yielding spin-distributions, state level splittings, and electronic densities of states consistent with prior hybrid functional calculations. Comparison of this detailed electronic structure with model Hamiltonian calculations suggests that the localized 3*d* iron moments induce correlation in the surrounding electron gas, strengthening local moment formation. This behavior is analogous to strongly correlated electronic systems such as Mott insulators, in which the GGA+*U* scheme serves as an effective single-particle representation for the full, correlated many-body problem. [http://dx.doi.org/10.1063/1.4755290]

I. INTRODUCTION

Iron porphyrins are widely represented in both naturally occurring and synthetic chemical systems, serving as a key site for redox chemistry. The breadth of this behavior is most apparent within the biological sphere, where the detailed role of the iron porphyrin is determined by the surrounding protein environment. While the overall architecture of this protein scaffold serves to tune nuances of the porphyrin electronic structure, the greatest modulation is induced by the amino acid residue ligating the metal center itself. In the case of a single histidine ligand, molecular oxygen may coordinate with iron for transport throughout an organism, as within hemoglobin and myoglobin. A more extreme case occurs in the catalases (phenolate ligand), peroxidases, and cytochromes P450 (thiolate ligand), in which molecular oxygen is activated and converted to either a hydroperoxo, peroxo, or oxyferryl reactive intermediate.[1] This particular oxyferryl radical cation, known as Compound I (Cpd I) is of great interest in its own right, serving as a potent oxidizing agent with a complex electronic state manifold.[2] A lucid theoretical picture for these particular porphyrins is of benefit not only for cytochrome P450 enzymology, but also to the study of other bioinorganic systems.

Inspired by these observations, several stable, biomimetic porphyrinato(thiolato)iron(III) complexes have been synthesized which undergo activation to an oxo iron(IV) porphyrin π-cation radical state.[3–5] Due to electronic donation from the thiolate, these species exhibit high catalytic activity toward substrate oxidation. Further advances in catalyst engineering have subsequently yielded yet more reactive porphyrin species, including those retaining this activity upon surface adhesion.[6] Consequently, the discussion herein will be concerned with these thiolate-ligated systems.

Previous density functional theory (DFT) and multireference calculations have canonically established that the low-lying states of Cpd I comprise a nearly-degenerate triradicaloid configuration (Figure 1).[2,7] Within this scheme, the π^*_{zx} and π^*_{zy} orbitals associated with the Fe=O unit are singly–occupied and couple to a third spin residing in an orbital comprising an admixture of porphyrin–centered a_{2u} and thiolate-centered p_σ(S) character. The ground state is generally accepted to be the $S = 1/2$ configuration, denoted $^2A_{2u}$, in which the $S = 1$ Fe=O unit is antiferromagnetically coupled to the $a_{2u} + p_\sigma$(S). Residing just above this is a second triradicaloid state, denoted $^4A_{2u}$, that possesses a ferromagnetic spin–spin coupling thereby affording a net $S = 3/2$ configuration. A second series comprise the $^{4,2}\Pi_S$ configurations in which the S=1 Fe=O unit is either ferromagnetically or antiferromagnetically coupled to a p_π(S) orbital. A $^{4,2}\Pi_S$ ground state configuration is nonetheless excluded by both theoretical[8] and experimental data, while the $^{2,4}A_{1u/2u}$ ground-state assignment is corroborated by experimental Raman,[9] Mössbauer, and electron spin-resonance spectroscopies of

a)jchackett@vcu.edu.

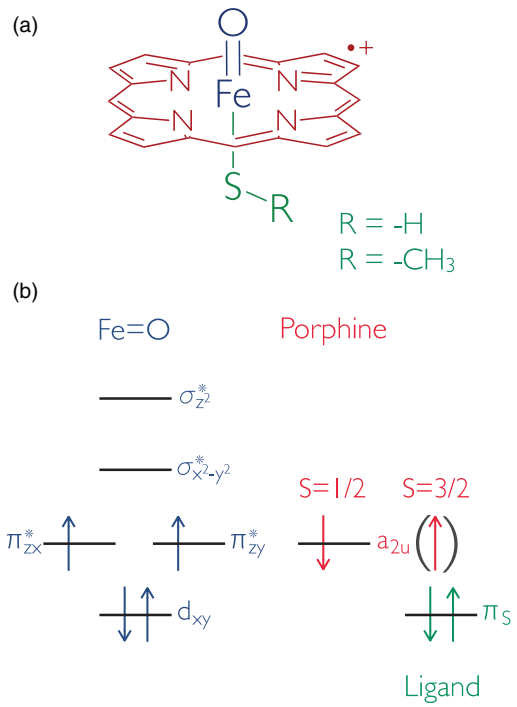

FIG. 1. (a) Truncated oxo-iron (IV) porphine model for thiolate-ligated Cpd I. (b) Consensus orbital structure of Cpd I as corroborated by theoretical and experimental studies.[2,7]

chloroperoxidase[10] and CYP119 (Ref. 11) Cpd I, as well as through internal consistency with theoretical calculations.[12]

The aforementioned theoretical calculations for Cpd I have largely utilized hybrid density functionals to treat correlated behavior at the metal center.[1,2] Hybrid functionals exhibit quantitative agreement with experiment and provide consistent predictions for reaction mechanism, however, the unsystematic nature of their development can obscure the physical processes underlying their predictions. An alternative treatment of electronic correlation is derived by augmenting the local density approximation (LDA) or generalized gradient approximation (GGA) to density functional theory with a localized site occupancy term at the metal center. The particular choice of this localizing potential is inspired by a model Hamiltonian for strongly correlated electron systems, specifically the Hubbard model.[13,14] This method, termed the DFT+U scheme,[15] allows realistic materials to be approached in a framework extending quantitatively beyond pure DFT while simultaneously retaining the transparency afforded by a toy model. Successes for DFT+U include reproduction of the correct band structure, density of states, and ground state symmetry for continuum semiconductors and doped Mott insulators[16] as well as isolated magnetic molecules.[17–22]

Herein, the DFT+U method is exploited to characterize the detailed electronic structure of thiolate-ligated Cpd I. This method provides unique insight into correlation physics while simultaneously benchmarking Cpd I electronic structure in a plane-wave pseudopotential schema. The latter point is particularly relevant for Car–Parrinello (CP)[23] and path-integral molecular dynamics,[24,25] which are most efficiently executed within this framework and are among the most valuable tools for *ab initio* molecular simulation. Such simulations have been previously performed for catalase and peroxidase Cpd I,[26–31] as well as solid-state species,[18,20–22,32–36] however, these were generally restricted to the GGA context. Accordingly, the calculations herein represent the first application of plane-wave DFT methods to thiolate-ligated porphyrins, and constitute the foundation for future explorations in systems such as the cytochromes P450. Recent accomplishments in materials chemistry likewise indicate that solid-supported porphyrins[6] serve as excellent oxidation catalysts, to which these DFT+U results are particularly germane.

II. THEORETICAL METHODS

A. GGA+U formalism

The DFT+U formalism represents the correlated physics of a many-body impurity system in a single particle framework. By virtue of its formulation, the bare GGA functional effectively contains a screened, mean-field representation of many-body behavior. To make these correlations explicit in DFT+U, the GGA energy is supplemented with a local moment term similar to that appearing in the Hubbard model[13,14] Hamiltonian, $E_{\mathrm{Hub}}[\{n^{I\sigma}_{mm'}\}]$. The doubly-counted GGA correlation $E_{\mathrm{DC}}[\{n^{I\sigma}\}]$ is then subtracted to give

$$E_{\mathrm{GGA+U}}[n(\vec{r})] = E_{\mathrm{GGA}}[n(\vec{r})] + E_{\mathrm{Hub}}\left[\{n^{I\sigma}_{mm'}\}\right] - E_{\mathrm{DC}}[\{n^{I\sigma}\}] \tag{1}$$

$$= E_{\mathrm{GGA}}[n(\vec{r})] + E_U\left[\left\{n^{I\sigma}_{mm'}\right\}\right]. \tag{2}$$

In this case, $n(\vec{r})$ is the spatial electron density and $n^{I\sigma}_{mm'}$ denotes the atom-centered spin-orbital occupation of the Ith atom on which the Hubbard correction is placed, as indexed by spin σ and angular momentum projection m. Since the doubly counted interactions are included in strictly a mean field sense, the term $E_{\mathrm{DC}}[\{n^{I\sigma}\}]$ depends solely on the net, spin-resolved orbital occupation $n^{I\sigma} = \sum_m n^{I\sigma}_{mm}$ in contrast to $E_{\mathrm{Hub}}[\{n^{I\sigma}_{mm'}\}]$.[15,37,38] A convenient representation for $n^{I\sigma}_{mm'}$ is obtained by projecting the valence electronic wavefunction ψ^σ_k with wavevector $\vec{k}$ and spin σ onto atom-centered spin orbital states ϕ^I_m so that $n^{I\sigma}_{mm'} = \sum_k f_k \langle\psi^\sigma_k|\phi^I_{m'}\rangle\langle\phi^I_m|\psi^\sigma_k\rangle$, with f_k the weight of the kth state.

The calculations herein are performed in a formalism that is invariant under rotation of the atomic orbital basis set defining the localized occupancies.[39,40] In this case, $E_{\mathrm{Hub}}[\{n^{I\sigma}_{mm'}\}]$ is determined by two free parameters: the screened on-site Coulomb interaction U and the exchange interaction J. To further simplify the problem, it is possible to absorb the exchange coupling J into the on-site term, $U_{\mathrm{eff}} = U - J$.[41] Physically, this corresponds to a neglect of the m_l dependence for U and does not differentiate between interaction strengths for ferromagnetically and antiferromagnetically coupled spin channels. In this case, the Hubbard correction to the Kohn–Sham functional assumes the form

$$E_U\left[\left\{n^{I\sigma}_{mm'}\right\}\right] = \frac{U}{2}\sum_I\sum_{m,\sigma}\left[n^{I\sigma}_{mm} - \sum_{m'} n^{I\sigma}_{mm'}n^{I\sigma}_{m'm}\right] \tag{3}$$

$$= \frac{U}{2}\sum_{I\sigma}\mathrm{Tr}[\hat{n}^{I\sigma}(1-\hat{n}^{I\sigma})]. \tag{4}$$

Introducing a set of localized orbitals diagonalizing the occupation matrices $\hat{n}^{I\sigma}$, the correction E_U simplifies considerably

$$E_U\left[\left\{n^{I\sigma}_{mm'}\right\}\right] = \frac{U}{2}\sum_{I\sigma}\sum_{i}\lambda_i^{I\sigma}\left(1-\lambda_i^{I\sigma}\right). \tag{5}$$

Quite clearly, this term is vanishing for either fully unoccupied ($\lambda_i^{I\sigma}=0$) or fully occupied ($\lambda_i^{I\sigma}=1$) configurations. Accordingly, the value U admits a physical interpretation as the additional energetic cost associated with assuming partial orbital occupancy ($\lambda_i^{I\sigma}\in(0,1)$). This term specifically corrects overcounting of the Coulomb self–interaction energy for partially occupied DFT orbitals as is inherent within the LDA and GGA approximations, thereby mimicking an open quantum system. In another sense, $E_U[\{n^{I\sigma}_{mm'}\}]$ may be viewed as eliminating the aberrant curvature of the GGA energy profile for cases of fractional orbital occupancy.

Viewing the Hubbard U term as a correction to the LDA/GGA, a natural choice of parameters is then to set U equal to the curvature of this energy functional, which can be obtained through a linear response method.[42] To accomplish this variational task, the single-particle potential V^{GGA} is perturbed to yield $V' = V^{GGA} + \sum_I \alpha_I P^I$, where α_I is the strength of the localized potential and P^I is a d-level projector for the Ith corrected atom. The problem may then be reduced to the minimization of total energy

$$E[\{q_I\}] = \min_{n(r),\alpha_I}\left[E[n(r)] + \sum_I \alpha_I(n_I - q_I)\right], \tag{6}$$

where α_I assumes the role of a Lagrange multiplier employed to enforce the orbital occupancy restraint. The Hubbard U term is then defined as

$$U = \frac{\partial^2 E[\{q_I\}]}{\partial q_I^2} - \frac{\partial^2 E^{GGA}[\{q_I\}]}{\partial q_I^2} \tag{7}$$

for a given initial orbital occupancy n_I, where the second term is subtracted to correct eliminate quadratic terms in E^{GGA} arising from processes other than electron-electron scattering. This subtraction may be physically interpreted as the resulting shift in electronic kinetic energy for all sites in the system due to the perturbation of the d-level electronic structure. Given that these contributions correspond to an overall background shift, they are not relevant for the determination of U.

For practical implementation, a Legendre transformation is performed, shifting dependence to the α_I parameter and thereby reducing the sum in (7) to a $\sum_I \alpha_I n_I$ term. The Hubbard U may then be written in terms of generalized susceptibilities $\chi_{IJ} = \partial n_I/\partial\alpha_J$ and $\chi^0_{IJ} = \partial n_I/\partial\alpha_J^{GGA}$, yielding

$$U = \left((\chi^0_{IJ})^{-1} + \chi^{-1}_{IJ}\right). \tag{8}$$

The bare susceptibility χ^0_{IJ} is accordingly derived by performing the DFT calculation at $\alpha_I = 0$ with fixed U_{in}, and the orbital occupancy response χ^0_{IJ} obtained through successive calculations at varying values of α_I using initial orbital occupancies from the bare calculation. The derived U then corresponds to a potential arising from redistribution of occupancies throughout the system subsequent to an induced perturbation on a d level and accompanying the electronic correlation at the perturbed site. This linear response approach is considerably easier to implement and more extensible than early constrained DFT methods for estimating U.[43] Since the choice of U_{in} is arbitrary, the corresponding linear response value U_{out} is dependent on the initial parameter set. Accordingly, it is useful to define a self-consistent U_{SCF} such that

$$U_{\text{SCF}} = U_{\text{out}} + \frac{1}{m}U_{\text{in}}, \tag{9}$$

where $m = (\sum_i(\alpha_i^I)^2)^{-1}$ is the effective degeneracy of the perturbed orbitals for all spin orbitals i. The self-consistent value U_{SCF} then corresponds to the electron–electron interaction present in the GGA functional component of the GGA+U state when $U = U_{\text{in}}$. Such a value is readily obtained through regression of several U_{out} values determined from U_{in} via the aforementioned scheme.[17]

B. Numerical details

Electronic structure calculations were performed using DFT and an ultrasoft pseudopotential (USPP) basis within the PWSCF module of the QuantumESPRESSO 4.2 suite.[44] All calculations were executed in the gas phase ($\epsilon = 1$) using a model system for Cpd I comprising either a thiolate (—SH) or methylthiolate (—SCH_3) axial ligand (Figure 1). Models were embedded in generously sized orthorhombic supercells, measuring 17.0 Å × 17.0 Å × 12.5 Å and 17.0 Å × 17.0 Å × 17.0 Å , respectively. The isolated, non-periodic nature of these systems eliminates the need for broad k-point sampling. Accordingly all physical quantities were calculated at the Γ point. Electronic states were converged to within 1.0×10^{-6} eV for both geometry optimizations and for pure SCF calculations. Geometry optimizations were performed for each value of the Hubbard U using a the CG/BFGS optimizer until the force on each atom was less than 0.005 eV Å^{-1}. The GGA to DFT was adopted and utilized in a spin-unrestricted context. Electronic structure was treated using the Perdew–Burke–Ernzerhof (PBE) density functional[45] with the semilocal approximation and a rotationally invariant GGA+U formalism.[42] In all cases, the gradient correction to the density was neglected when the electronic density itself was less than $1.0\times10^{-6}\ ea_0^{-3}$. USPP calculations were executed using Vanderbilt pseudopotentials,[46] a plane wave kinetic cutoff of 30 Ry, and a charge-density cutoff at 240 Ry. A Gaussian smearing factor of 0.14 eV was utilized for Fermi level estimations.

Reference calculations within a Gaussian-type orbital (GTO) scheme were performed for both model systems. Calculations were conducted using the ORCA 2.7 package[47] in conjunction with the PBE functional and def2-TZVP basis[48] on all atoms. Additional calculations using the PBE0 (Ref. 49) functional were likewise performed with the def2-TZVP basis and the TURBOMOLE 5.10 (Ref. 50) package, as ORCA was unable to converge the $S = 1/2$ systems to their proper triradicaloid ground state. Atomic spin densities for both plane-wave and GTO cases were determined using volumetric spin difference density profiles and Voronoi triangulation as implemented in the Bader 0.27 code.[51–53] Volumetric data were

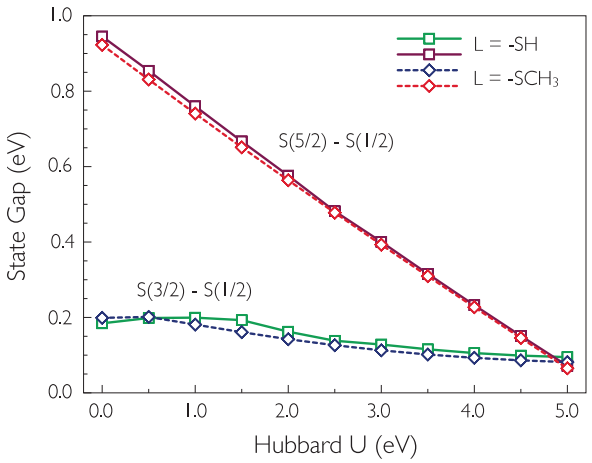

FIG. 2. Relative spin-state energetics obtained by utilizing the Hubbard U as a fitting parameter. The solid line and squares correspond to the thiolate axial ligand, whereas the dashed line and diamonds correspond to the methylthiolate axial ligand.

calculated using a mesh with resolution equal to the number of grid points comprising the finest Fourier grid in the corresponding plane-wave DFT calculations (typically 180 × 180 × 128 real space mesh points).

III. DISCUSSION

In order to reconcile GGA+U calculations with prior GGA and hybrid functional data for Cpd I, U was treated as both a self-consistently determined parameter and as a tunable parameter. Three properties were exploited to assess the degree of consistency with prior experimental and theoretical data: spin-state dependent energy splittings, spin-density distributions, and molecular geometries.

A. Empirical determination of Hubbard *U* for Cpd I

The most straightforward metrics for the electronic structure of Cpd I are the relative energetics of different spin states. As the effective value of U is increased, both the $\Delta E_{3/2\rightarrow 1/2}$ gap and the $\Delta E_{5/2\rightarrow 1/2}$ gap are observed to decrease in a nearly linear manner in both model systems (Figure 2). Of these, the $\Delta E_{5/2\rightarrow 1/2}$ state gap decreases most rapidly. All values of U lying below 5.0 eV correspond to a state ordering consistent with existing DFT and multireference calculations,[7] in which progressively higher spin states lie progressively higher in energy. A spin-state crossover occurs for $U > 5.0$ eV, whereupon the ground state assumes a sextet configuration. For larger values of U, geometry optimizations generally failed to converge and hence no systematic exploration of these configurations was attempted. Electron paramagnetic resonance data for chloroperoxidase[10] and cytochrome P450–119 Cpd I (Ref. 11) support the determination of a $S = 1/2$ ground state, consistent with these calculations.

Choosing an optimal Hubbard U lying between 3.0 and 4.0 eV generates a $\Delta E_{5/2\rightarrow 1/2}$ splitting consistent with the predictions of hybrid DFT calculations employing the PBE0 density functional. Nonetheless, the $\Delta E_{3/2\rightarrow 1/2}$ splitting remains larger than the hybrid DFT value, with the latter calculations suggesting that these states are nearly degenerate (Table I). The resulting gap is nonetheless smaller than the GGA value, and yet larger than the PBE0 result within chemical accuracy. While the choice of U is system-dependent, it is notable that the same optimal range reproduces both experimental and theoretical data in prior GGA+U studies of iron-porphyrins.[18,20–22,54,55] Interestingly, the energetic splittings do remain comparable between the pseudopotential plane-wave and all-electron localized–orbital basis schemes for all considered points of comparison. The semilocal approximation accordingly appears to afford a sufficient treatment of core-level effects systems like Cpd I in which the relevant electronic states lie proximate to the Fermi level.

With respect to geometric parameters, a high degree of similarity is observed between GGA based-schemes irrespective of the basis employed or the choice of axial ligand. Among density functionals, PBE calculations provide bond distances with a slightly tighter calibration to experimental extended x-ray absorption fine structure (EXAFS) data for chloroperoxidase Cpd I than does its hybrid counterpart PBE0.[56] As the value of U is increased from $U = 0.0$ eV to $U = 3.5$ eV, the bowed or twisted ring geometries obtained using the PBE functional become more planar, resembling those obtained at the PBE0 level. Some degree of deformation from planarity is essential as symmetry breaking below $C2$ is requisite for the productive overlap between Fe=O e_g (d_{zx} and d_{zy}) orbitals and the porphine a_{2u}, and hence the antiferromagnetic coupling observed in the $S = 1/2$ state.[57] This, in turn, stabilizes a ferromagnetic spin configuration for the quartet state by supporting spin accumulation on porphine nitrogens.

The Fe—S distance calculated with the PBE functional increases by 0.03 Å for the thiolate and by 0.05 Å for the methylthiolate ligand in the $S = 1/2$ ground state when U is increased to $U = 3.5$ eV, concurrent with deviation of the porphine from a planar configuration. A similar shift is observed in the $S = 3/2$ configuration, with the PBE distances increasing by 0.03 Å and 0.04 Å , respectively. The Fe=O and mean Fe—N distances undergo little alteration as U is increased, while no variation whatsoever is observed for any geometric parameter in the $S = 5/2$ state. This behavior can be attributed to a decrease in Fe—S bonding character for the $S = 1/2$ and $S = 3/2$ states, concomitant with a rearrangement of the low-lying virtual orbital structure within the Fe=O unit. Finally, it is notable that the Fe—S bond distances calculated with the hybrid PBE0 functional are uniformly ∼0.10 Å longer than the corresponding PBE derived bond lengths.

The spin-density distribution and magnetization profile exhibit a pronounced redistribution concurrent with the scaling of U. Notably, the absolute cell magnetization, $M_a = \int_{\mathcal{V}} |\rho_\uparrow(\vec{r}) - \rho_\downarrow(\vec{r})|\, d\vec{r}$, exhibits a positive, linear correlation with U for the $S = 1/2$ state, irrespective of the axial ligand (Figure 3). This behavior is not observed in either the $S = 3/2$ and $S = 5/2$ states. Physically, this scaling corresponds to a strengthening of antiferromagnetic correlations; behavior which in fact should not be observed in the ferromagnetically coupled $S = 3/2$ and $S = 5/2$ configurations. Accompanying

TABLE I. Calculated geometric and energetic parameters for model thiolate-ligated Cpd I systems and corresponding experimental EXAFS geometric data for chloroperoxidase (CPO) Cpd I.[56]

Ligand	Functional (Hubbard U)	Spin state	Fe—O (Å)	Fe—S (Å)	Fe—N[a] (Å)	Energy (eV)
—SH						
	PBE (0.0 eV)					
		$S = 1/2$	1.64	2.34	2.02	…
		$S = 3/2$	1.67	2.44	2.00	0.184
		$S = 5/2$	1.66	2.48	2.08	0.945
	PBE (3.5 eV)					
		$S = 1/2$	1.65	2.37	2.02	…
		$S = 3/2$	1.66	2.47	2.02	0.116
		$S = 5/2$	1.66	2.48	2.09	0.316
	PBE (GTO)					
		$S = 1/2$	1.64	2.35	2.02	…
		$S = 3/2$	1.67	2.45	2.00	0.188
		$S = 5/2$	1.65	2.48	2.08	1.092
	PBE0 (GTO)					
		$S = 1/2$	1.61	2.53	2.00	…
		$S = 3/2$	1.61	2.54	2.00	0.010
		$S = 5/2$	1.61	2.57	2.07	0.337
—SCH_3						
	PBE (0.0 eV)					
		$S = 1/2$	1.65	2.33	2.02	…
		$S = 3/2$	1.67	2.45	2.01	0.199
		$S = 5/2$	1.66	2.51	2.08	0.923
	PBE (3.5 eV)					
		$S = 1/2$	1.65	2.38	2.02	…
		$S = 3/2$	1.66	2.49	2.02	0.102
		$S = 5/2$	1.66	2.51	2.09	0.309
	PBE (GTO)					
		$S = 1/2$	1.64	2.35	2.02	…
		$S = 3/2$	1.66	2.47	2.02	0.192
		$S = 5/2$	1.65	2.51	2.08	1.070
	PBE0 (GTO)					
		$S = 1/2$	1.61	2.56	2.01	…
		$S = 3/2$	1.61	2.57	2.00	0.008
		$S = 5/2$	1.61	2.61	2.07	0.343
EXAFS[b]			1.65	2.48	2.01	

[a]Mean values are provided for Fe–N distances.
[b]Uncertainties in the reported EXAFS data are ±0.02 Å.

the increase in $S = 1/2$ magnetization is a substantial, monotonic spin-density accumulation on the Fe=O unit (Figure 4). The antiferromagnetically coupled minority spin population undergoes a crossover from ligand-centered to porphine-centered character at approximately $U = 3.5$ eV for the thiolate system. The methylthiolate likewise experiences an increase in Fe=O spin polarization, however, the accompanying ligand and porphine densities do not cross, with the radical remaining ligand-centered. Throughout this process the spatial spin–density distribution and symmetry remain consistent between both ligands, exhibiting a characteristic "Cpd I" configuration (Figure 5). The nature of the radical character is system dependent, with EPR[10] and ENDOR[58] for chloroperoxidase Cpd I supporting a porphyrin-centered $S = 1/2$ ground state. Conversely, EPR characterization of CYP119 Cpd I supports a ligand-centered $S = 1/2$ ground-state radical configuration.[11]

In contrast, the $S = 3/2$ state exhibits a biphasic spin-density profile, comprising an initial drop in Fe=O

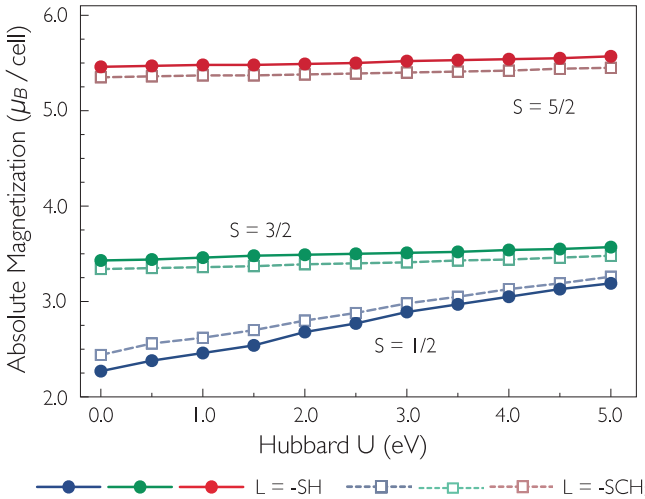

FIG. 3. Increase in net cell magnetization induced by increasing U for three distinct spin states (doublet: blue; quartet: green; sextet: red) and for each axial ligand (thiolate: filled circles; methylthiolate: hollow squares).

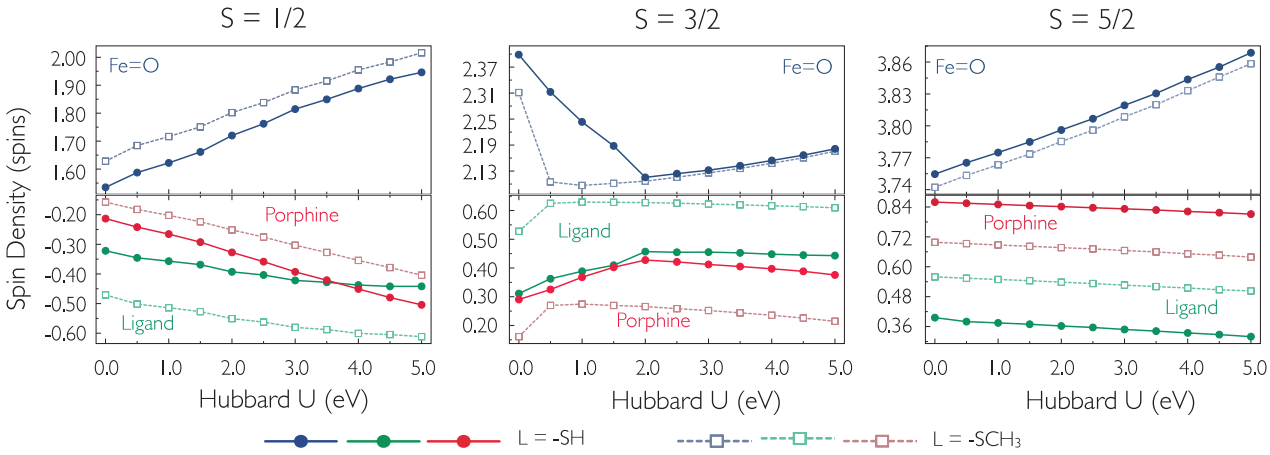

FIG. 4. Scaling of group spin density with increasing Hubbard U for Fe-O, porphine, and ligand subunits of Cpd I (Fe=O: blue; porphine: red; ligand: green) as delimited for each axial ligand (thiolate: filled circles; methylthiolate: hollow squares).

polarization accompanied by an increase in the ferromagnetically coupled spin population on both the ligand and the porphine upon variation of U (Figure 4). During this phase, the spin-density for the thiolate system is almost evenly partitioned between the axial ligand and the porphine, with a slight excess retained on the porphine. When $U > 2$ eV for the thiolate ($U > 1.0$ eV for the methylthiolate) the spin density on Fe=O begins to gradually increase, while the combined ligand and porphine spin density diminishes. Furthermore, for the thiolate, the ligand-porphine spin density gap increases with the ligand acquiring a small but nonzero addition of radical character. The methylthiolate does not exhibit this behavior, with spin density overwhelmingly distributed on the axial ligand for all values of U. The high–spin $S = 5/2$ configuration exhibits the most uniform scaling. In this case, the spin density on the Fe=O gradually increases while that on the remainder of the system monotonically decreases, reflecting a slight increase in spin localized on the Fe=O unit. The same behavior is observed for both axial ligands, with the largest spin-density gap obtained for the thiolate system accompanied by a consistent ligand-centered radical character.

It should be noted that prior DFT calculations suggest this radical distribution is highly sensitive to environmental effects, adopting a ligand-centered character for the gas-phase methythiolate or the cysteineate without hydrogen bonding. This character in turn shifts to an evenly partitioned radical for the thiolate and the cysteinate/methylthiolate with hydrogen bonding or in the presence of even a slight dielectric background.[2] Irrespective of these limitations, the $S = 1/2$ models with U lying between 3.0 eV and 4.0 eV appear to comprise a tunable, consistent representation of experimentally observed Cpd I systems.

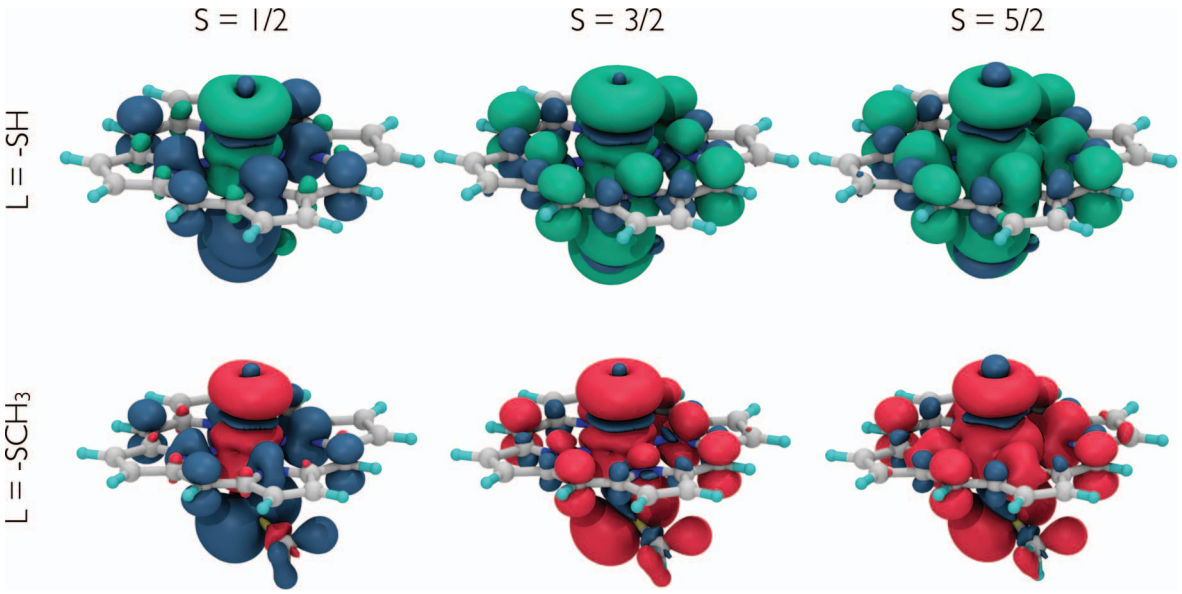

FIG. 5. Spatial spin difference density distributions for thiolate and methylthiolate systems with $U = 3.5$ eV (majority spin population: green/red; minority spin population: blue). Note the distinct antiferromagnetic triradicaloid configuration assumed by the doublet and the ferromagnetic triradicaloid configuration assumed by the quartet. Contours are drawn at ±0.001 a.u.

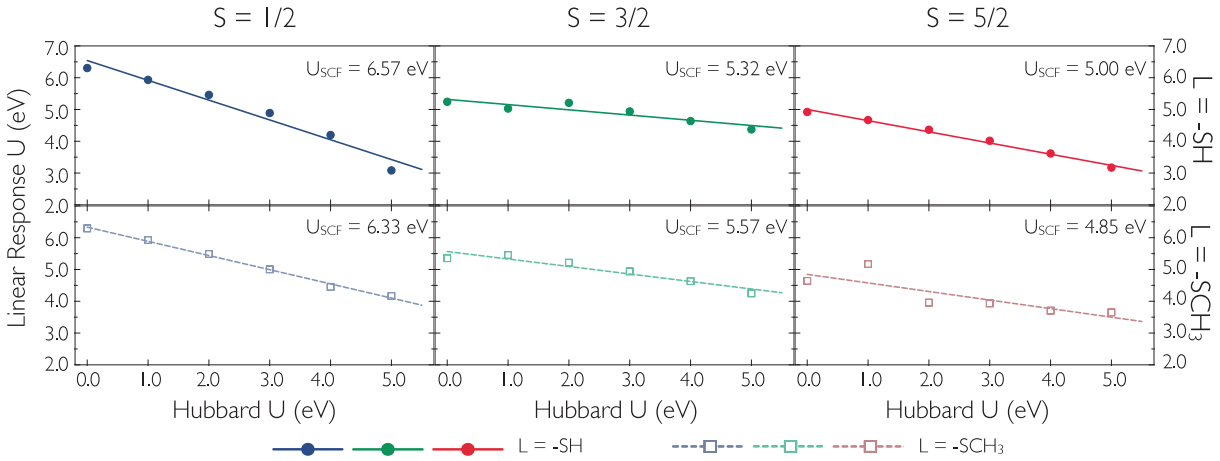

FIG. 6. Linear response determination of individual U values and U_{SCF} in distinct spin states (doublet: blue; quartet: green; sextet: red) and for each axial ligand (thiolate: filled circles; methylthiolate: hollow squares).

B. Self-consistent determination of Hubbard *U*

The GGA+U formalism is an attractive alternative to the use of hybrid density functionals as a means to circumvent the poor treatment of electron localization in correlated systems due to excess Coulomb self-interaction error inherent in GGA functionals. In this case, a consistent algorithm to determine a physically meaningful value of U is highly desirable. To this end, a linear-response based method for the self-consistent determination of $U = U_{SCF}$ was exploited, using the geometries calculated during the empirical determination.[17] The values of U_{SCF} obtained through this regression method are significantly larger than those obtained by empirically fitting experimental and theoretical data (Figure 6). In all cases excepting the methylthiolate $S = 5/2$ state, the resultant U was greater than 5.0 eV. Empirical scaling calculations indicate that this value lies beyond a spin-state crossing in which the $S = 5/2$ state becomes the ground state of the system. While still a relatively low-lying state, the high-spin pentaradicaloid is nonetheless established to reside notably higher in the state manifold than the $S = 1/2$ or $S = 3/2$ states[7,12,59,60] and hence this determination contradicts established experimental and theoretical data. Furthermore, converged geometries were difficult or impossible to obtain for values of $U > 5.0$ eV, suggestive of an electronic structure instability in this regime. While the linear response method for determination of U_{SCF} has proven relatively successful for simple diatomic systems,[17,19,61] this method has been shown to overestimate U_{SCF} for more complex systems, including model porphyrins.[18] These calculations corroborate such observations.

C. Bonding and electronic structure of Cpd I

1. GGA electronic configuration of S = 1/2 Cpd I (U = 0.0 eV)

Given that the $S = 1/2$ and $S = 3/2$ states are presumed to dominate the catalytic activity of Cpd I, a detailed discussion of electronic structure is provided only for these species. With respect to localized electronic structure of Cpd I, the thiolate and methylthiolate porphines have a nearly-indistinguishable total density of states (DOS) in the Fe($3d$) channel at $U = 0.0$ eV in the $S = 1/2$ configuration (Figure 7). In particular, no states occupy the Fermi level E_F for either axial ligand. Furthermore, only a small gap of 0.66 eV exists in the spin-majority channel between the HOMO and LUMO. Analysis of the m_l projected density of states (pDOS) for the thiolate-ligated porphine indicates that the HOMO state comprises an admixture of all five $3d$ angular momentum channels, with d_{z^2}, d_{zy}, and $d_{x^2-y^2}$ character predominating. The spin-majority LUMO is more simplistic, of largely $d_{x^2-y^2}$ character, followed by a spin-minority state 0.70 eV above E_F with a similar composition to the HOMO. Retaining a $S = 1/2$ spin configuration and shifting to the methylthiolate ligand, the states lying near the HOMO assume a configuration dominated by d_{zx}, d_{zy}, and $d_{x^2-y^2}$ spectral components. Relative to the thiolate system, d_{zx} spectral weight is redistributed from states lying below E_F so that the d_{z^2}, d_{zx}, and d_{zy} are in turn distributed with equal weight near the Fermi energy.

Particularly notable during the exchange of ligands is a loss of spectral weight from the d_{zx} states in majority and minority spin populations lying −1.26 eV and −0.91 eV below E_F, respectively. This is accompanied by an accumulation in these populations for states lying at −0.36 eV below E_F (majority) as well as at 0.70 eV (minority), 1.74 eV (majority), and 2.00 eV (minority) above E_F. Consequently, the $S = 1/2$ methylthiolate is a configuration in which d_{zx} and d_{zy} spectral components are partitioned in equal proportion within peaks above and below the Fermi level. This arrangement is highly consistent with the accepted theoretical picture of Cpd I in which a pair of individual spins reside in degenerate singly-occupied π^*_{zx} and π^*_{zy} orbitals on the Fe=O unit. These orbitals are themselves comprise bonding-antibonding pairs that emerge from hybridization of Fe($3d_{zx}$)–O($2p_x$) and Fe($3d_{zy}$)–O($2p_y$) atomic orbitals (Figure 1). Corroborating this assignment is the overlap of the O($2p$) pDOS with $3d_{zx}$ and $3d_{zy}$ spectral weight (Figure 7 vs. Figures 8 and 9), and the even partition of states above and below E_F for these half-occupied virtual channels. Furthermore, substantial overlap exists between Fe($3d$) states lying at −1.51 eV, −1.26 eV, and −0.36 eV and the N($2p$), O($2p$), and S($2p$), accounting for the delocalized radical character of the system.

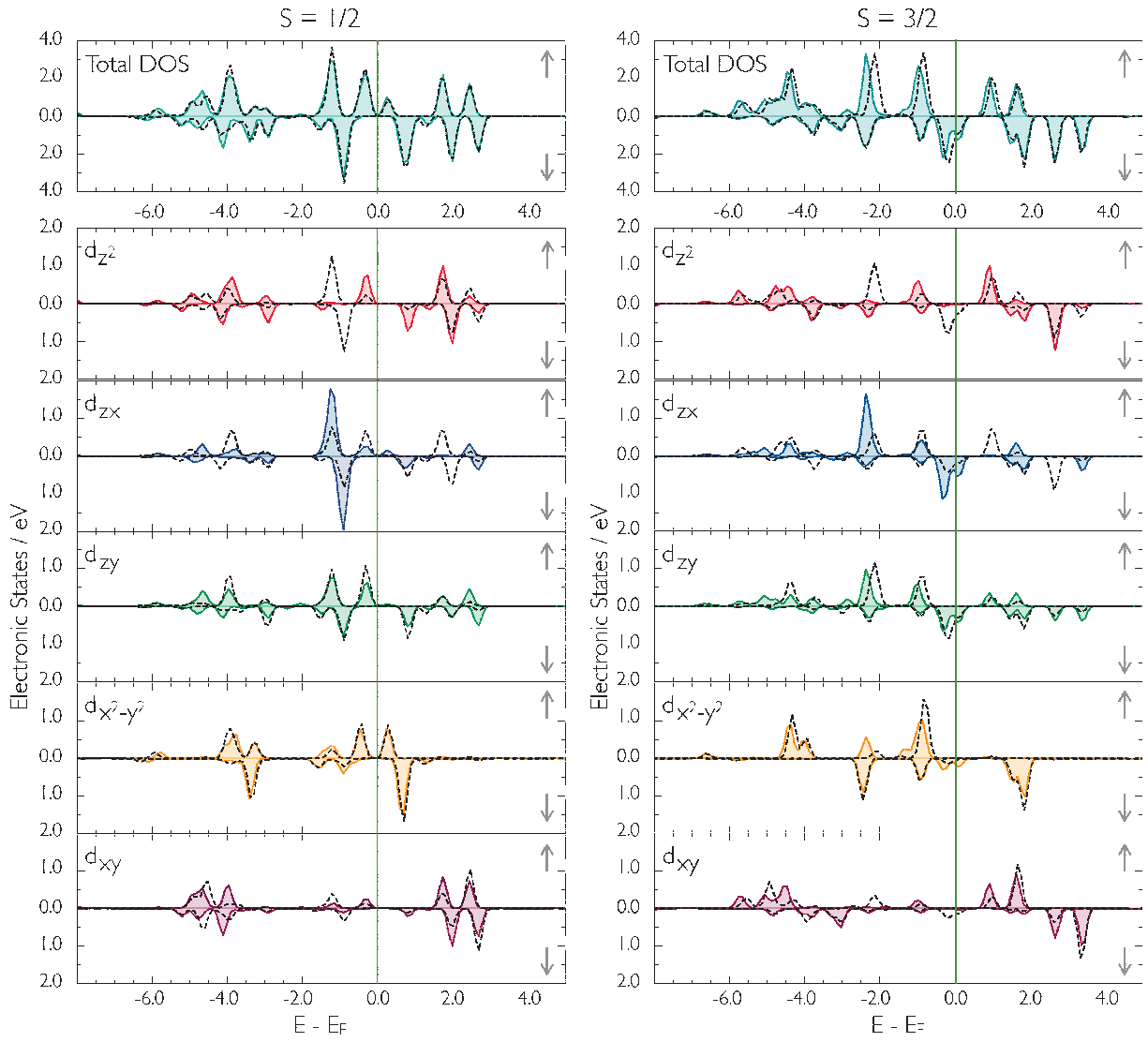

FIG. 7. Electronic density of states for thiolate (filled) and methylthiolate (dashed) model systems as calculated with $U = 0.0$ eV in the two lowest-lying spin states (total DOS: teal; d_{z^2} pDOS: red; d_{zx} pDOS: blue; d_{zy} pDOS: green; $d_{x^2-y^2}$ pDOS: yellow, d_{xy} pDOS: purple).

The methylthiolate is accordingly distinguished from the thiolate by diminished overlap between the S(2p) and Fe(3d) DOS at −0.91 eV, decoupling axial electronic states from the metal center and hence promoting localization at this site.

Progressing away from the immediate vicinity of E_F are a set of states at 1.74 eV and 2.00 eV with d_{xy} and d_{z^2} character, as observed for both the $S = 1/2$ thiolate and methylthiolate (Figure 7). These states likewise contain a weak d_{zy} component for both ligands, which is accompanied by an additional d_{zx} component via the aforementioned spectral shift in the case of the methylthiolate. The highest lying states occur at 2.44 eV (majority) and 2.70 eV (minority) in which an admixture of character from all m_l channels except $d_{x^2-y^2}$, however, d_{xy} strongly predominates. In the case of the methylthiolate the high-lying states are accompanied by an additional prominent d_{z^2} component. This outlying spectral configuration may accordingly be assigned to the σ^*_{xy} and $\sigma^*_{z^2}$ virtual orbitals. Notably, these states overlap with O(2p) and S(2p) spectral weight, consistent with a picture in which the Fe(d_{z^2}) hybridizes with the O($2p_z$) and S($2p_z$) to form a metal-ligand bond (Figure 7 vs. Figures 8 and 9). The virtual orbital structure lying near and above E_F establish states into which an electron may be promoted or from which it may be donated, affording a perspective on electronic mobility in Cpd I. Conversely, states lying below E_F establish bonding patterns and hence structural parameters of the system. This pattern is readily apparent upon examination of the heavy orbital overlap between the Fe(3d) pDOS and the ligand states lying below −2.00 eV in both spin channels (Figure 7).

2. GGA electronic configuration of S = 3/2 Cpd I (U = 0.0 eV)

The $S = 3/2$ configurations for both ligands are characterized by projected densities of states which are similar in content to those of the $S = 1/2$ spin configuration. Nonetheless, notable deviations do exist. In particular, the $S = 3/2$ systems are distinguished by the presence of states overlapping E_F in the $S = 3/2$ spin-minority channel

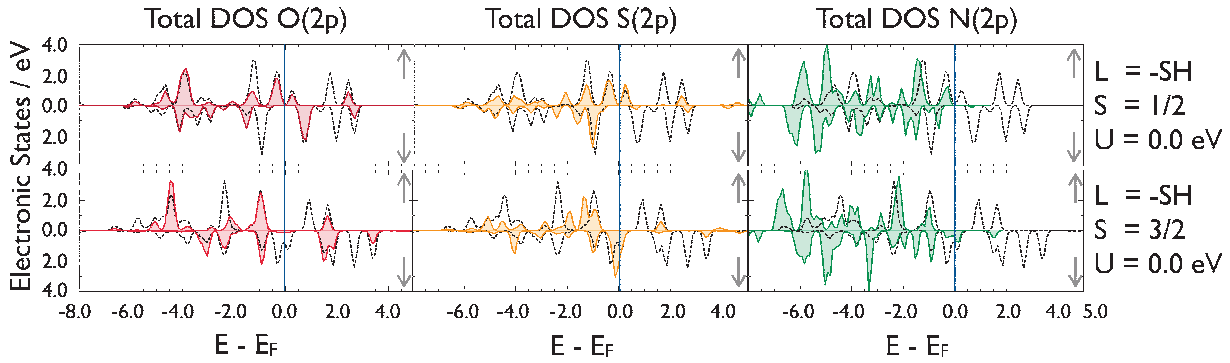

FIG. 8. Overlap between total thiolate Fe(3*d*) density of states (dashed) and the total density of states for coordinating species (oxygen: red fill; ligand sulfur; yellow fill; porphine nitrogens: green fill) for doublet and quartet spin states with $U = 0.0$ eV.

(Figure 7). For either ligand, these states are an admixture of d_{zx} and d_{zy} character, with this distribution becoming more symmetric for the methylthiolate in a manner paralleling the $S = 1/2$ case. These states likewise acquire a large d_{z^2} and minor d_{xy} weight when shifting from the thiolate to the methylthiolate. A small $d_{x^2-y^2}$ component is observed in either case. The maxima of these states are proximate to E_F, residing at −0.33 eV and −0.07 eV for either ligand.

Below E_F are found two pairs of states with proximate maxima in both $S = 3/2$ spin channels. Referring to the thiolate ligand, the first pair occurs at at −2.43 eV (majority)/−2.37 eV (minority) with d_{zx} and d_{zy} weight dominating in the spin majority and $d_{x^2-y^2}$ in the spin minority channel. These states acquire a notable majority d_{z^2} component when exchanging the thiolate for the methylthiolate, accompanied by an even redistribution of spectral weight to the d_{zx} and d_{zy} states proximate to E_F and a loss of the majority $d_{x^2-y^2}$ component. This is accompanied by a slight upward shift of these majority channel states toward E_F for the methylthiolate ligand. The second set of states at −0.97 eV (majority)/ −0.93 eV (minority) are more diverse, containing a contribution from all 3*d* angular momenta with the $d_{x^2-y^2}$ dominant followed by an equal mixture of d_{z^2}, d_{zx}, and d_{xy}. By analogy with the $S = 1/2$ system, these states may be tentatively identified with the partially-occupied π^*_{zx} and π^*_{zy} virtual orbitals, with a minor contribution from the $\sigma_{x^2-y^2}$, as a consequence of hybridization with porphine states (Figures 8 and 9). States lying below −2.00 eV contain a mixture from all m_l channels, again corresponding to predominantly bonding configurations (Figure 7).

The nature of states lying above the Fermi level differs significantly between $S = 1/2$ and $S = 3/2$ systems. Nonetheless, several parallel trends between these systems allow general inferences to be drawn. For the $S = 3/2$ thiolate, a spin-majority state is found 0.93 eV above E_F, comprising solely d_{z^2} and d_{xy} character alongside minor d_{zy} components. A similarly uneven distribution of spectral components was seen at 0.80 eV for the $S = 1/2$ thiolate (Figure 7), albeit with different m_l channels. Upon a shift from the $S = 3/2$ thiolate to methylthiolate, spectral weight is redistributed from the majority −2.37 eV state to this state and that lying at −0.97 eV, again effecting an even partition of spectral weight from d_{zy} and d_{zx} components within a given DOS peak. This behavior is again observed for both the $S = 1/2$ and $S = 3/2$ states, suggesting that one effect of the methylthiolate ligand is to ensure an even spin partition between these channels. While it is tempting to associate the 0.93 eV state directly with the π^*_{zx} and π^*_{zy}, strong d_{z^2} character likewise suggests association with a low-lying $\sigma^*_{z^2}$ virtual orbital.

Progressing further from the Fermi level to 1.74 eV, a state is found in the majority channel with major d_{xy} character and minor d_{zx}/d_{zy} contributions, accompanied by an overlapping spin minority pair at 1.47 eV and 1.87 eV of largely $d_{x^2-y^2}$ character. Referring to the orbital structure of Cpd I (Figure 1), the majority channel states may be associated with the unoccupied σ^*_{xy} orbital, and the minority channel states

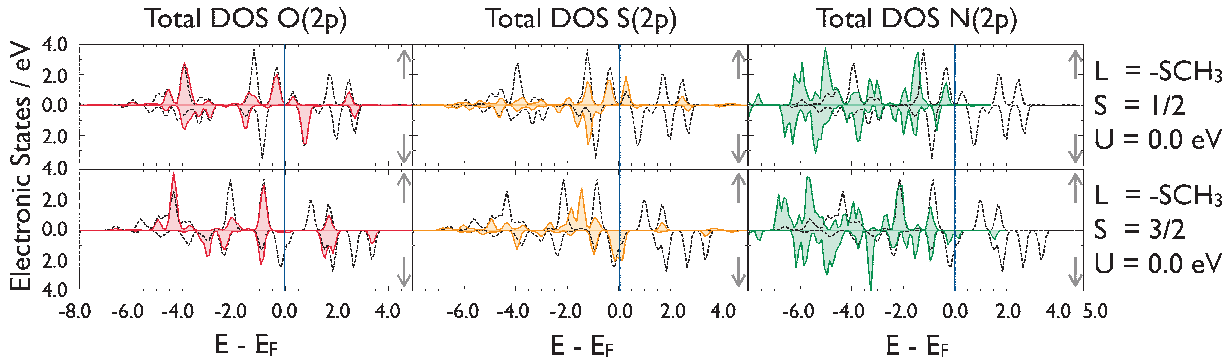

FIG. 9. Overlap between total methylthiolate Fe(3*d*) density of states (dashed) and the total density of states for coordinating species (oxygen: red fill; ligand sulfur; yellow fill; porphine nitrogens: green fill) for doublet and quartet spin states with $U = 0.0$ eV.

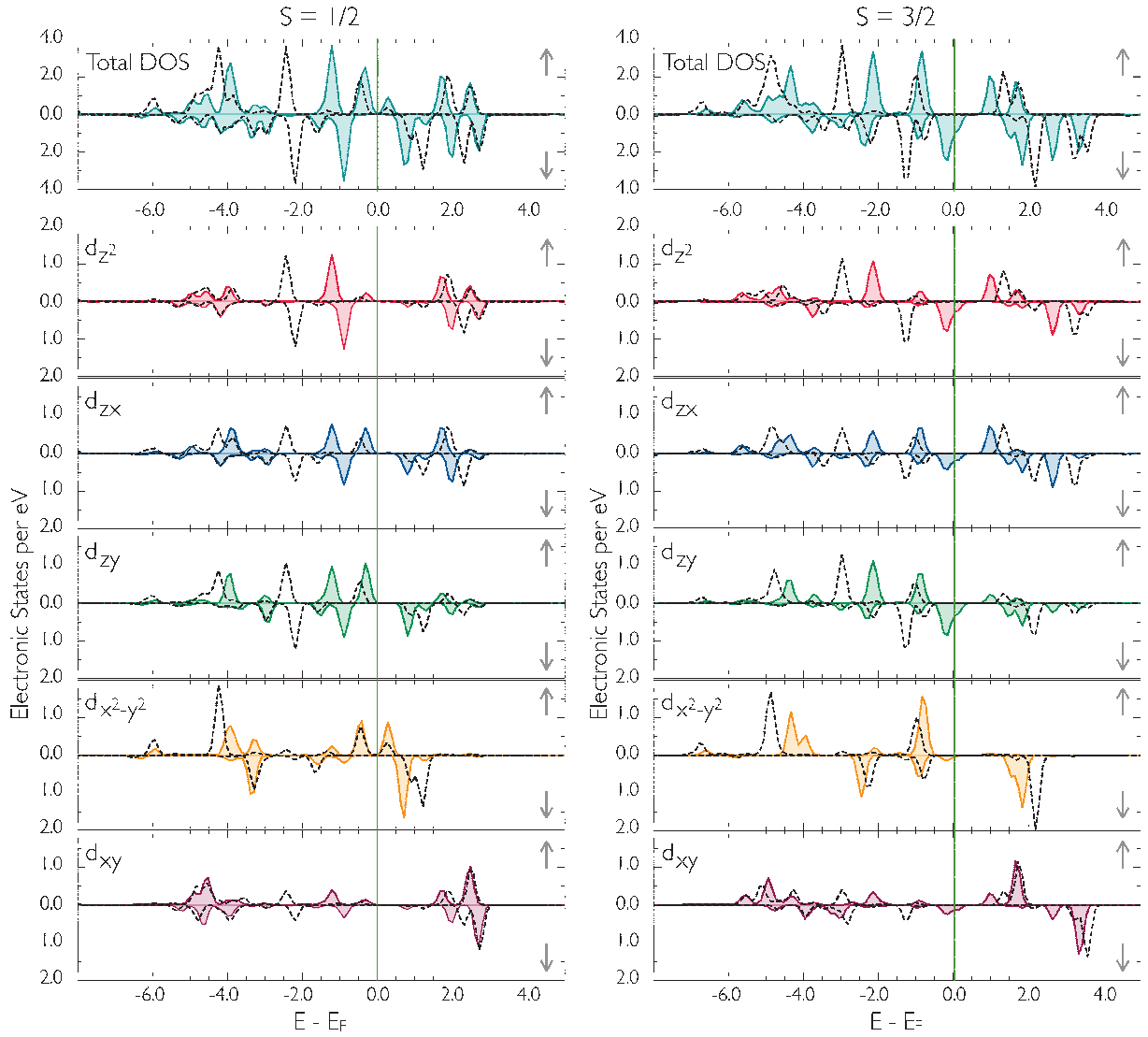

FIG. 10. Electronic density of states for the methylthiolate model system in the lowest spin-states, calculated in $U = 0.0$ eV (filled) and $U = 3.5$ eV (dashed) configurations (total DOS: teal; d_{z^2} pDOS: red; d_{zx} pDOS: blue; d_{zy} pDOS: green; $d_{x^2-y^2}$ pDOS: yellow; d_{xy} pDOS: purple).

associated with the $\sigma^*_{x^2-y^2}$. The remaining spin-minority states at at 2.67 eV and 3.37 eV above E_F are an admixture of d_{z^2} and d_{xy} character. These states likewise comprise small d_{zx} and d_{zy} components, with an uneven partition of spectral weight between the two. As in all other cases, this distribution is equalized when shifting from the thiolate to the methylthiolate ligand (Figure 7). Following the preceding argument, these states may be associated with a combination of $\sigma^*_{z^2}$ and σ^*_{xy} virtual orbitals, with the 2.67 eV state predominating in the $\sigma^*_{z^2}$ orbital and the 3.37 eV state in the σ^*_{xy} orbital.

With respect to the Fe coordination sphere, the σ^*_{xy}–like state at 1.74 eV overlaps strongly with the O(2p) and and to a lesser extent the S(2p) DOS contributions above E_F (Figures 8 and 9). The O(2p) likewise coincides with the putative $\sigma^*_{x^2-y^2}$ and the π^*_{zx} / π^*_{zy}, suggesting a more complicated electronic arrangement between the metal center and the axial ligands than is present in the $S = 1/2$ case. This is corroborated by coincidence between porphine states above E_F and the $\sigma^*_{x^2-y^2}$, as well as mutual overlap between the π^*_{zx} and π^*_{zy} and the ligand pDOS at all energies. This admixture across Fe(3d) states may be due to the indistinguishable porphine a_{2u} spin and axially–centered virtual π^*_{zx} and π^*_{zy} spins inherent for the single-reference representation provided by DFT.

3. Electronic structure for finite Hubbard U (U = 3.5 eV)

Having established the detailed pDOS of Cpd I in the presence of the correlation inherent in the GGA functional, it is possible to ascertain the effect of the Hubbard U parameter on this system. This correction induces a distinct perturbation of the 3d electronic structure, generally shifting states below E_F to lower energies and states above E_F to higher energies (Figure 10). The methylthiolate-ligated porphine is explicitly utilized for discussion, as this species suitably reproduces a porphyrin with a symmetric π^*_{zx} / π^*_{zy} configuration and ligand-centered radical character. Nonetheless, these conclusions apply equally well to the thiolate configuration (supplementary material, Figure 1 (Ref. 62).

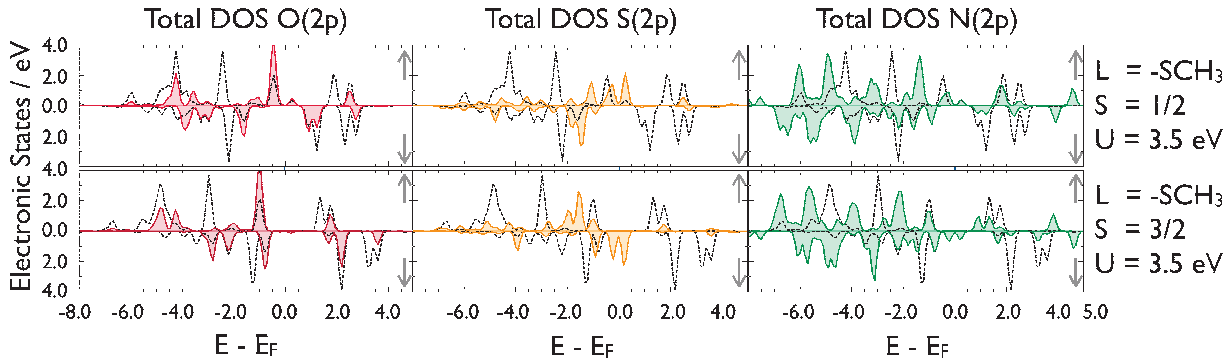

FIG. 11. Overlap between total methylthiolate Fe(3*d*) density of states (dashed) and the total density of states for coordinating species (oxygen: red fill; ligand sulfur; yellow fill; porphine nitrogens: green fill) for doublet and quartet spin states at finite $U = 3.5$ eV.

As U is increased from 0.0 eV to 3.5 eV, the $S = 1/2$ majority (minority) states at -1.22 (-0.89 eV) shift away from E_F by -1.22 eV (-1.29 eV) (Figure 10). This behavior is localized almost entirely within the d_{z^2}, d_{zx}, and d_{zy} channels. Accompanying these rearrangements are numerically less significant displacements of states above E_F to higher energies, notably of the state at 0.71 eV comprising $d_{x^2-y^2}$, d_{zx}, and d_{zy} character and the states at 1.68 eV and 2.01 eV of d_{z^2}, d_{zx}, and d_{zy} character. This process serves to widen the gap between occupied and unoccupied 3*d* components of the π^*_{zx} / π^*_{zy} pair, thereby enhancing the tendency to favor either completely occupied or unoccupied orbital configurations, much as the Mott insulator state is realized in the Hubbard model.[14] Concomitant is a redistribution of spectral overlap between the O(2*p*) with d_{zx} and d_{zy} states below E_F to those components lying above E_F indicating a shift between electron and hole distributions on the Fe=O unit (Figure 11 vs Figure 10) and hence local moment formation. This process diminishes the overlap between the d_{zx} / d_{zy} states below the Fermi level and the S(2*p*) DOS, which may be taken as a hallmark of increasing spin localization on the axial methylthiolate.

The low-lying $\sigma^*_{x^2-y^2}$ and $\sigma^*_{z^2}$ like states above E_F, which serve as acceptors for a promoted electron in the pentaradicaloid $S = 3/2$ configuration,[60] undergo a similar pattern of displacement. Following this argument, it is significant that the bonding σ_{xy} and antibonding σ^*_{xy} are essentially unchanged. This observation is sensible in light of the bonding configuration between σ_{xy} and the porphine system, and the correspondingly high-lying nature of the σ^*_{xy}. The porphine N(2*p*) DOS itself is redistributed to a configuration above E_F with a near universal overlap of the Fe(3*d*) DOS, as well as to a pair of high-lying states with no overlap whatsoever (Figures 9 and 11).

The spectral changes observed for the $S = 3/2$ configuration parallel those of the $S = 1/2$ state, excepting the unique circumstances inherent in the spin-minority states lying at E_F. In this case, the corresponding spectral weight is shifted to a pair of states in the same spin channel, displaced below E_F to -1.31 eV (Figure 10). Interestingly, the N(2*p*) spectral weight coinciding with these states is retained at E_F, as are the minor contributions from the O(2*p*) and S(2*p*) DOS (Figure 11). Also significant is a loss of spectral overlap between the N(2*p*) DOS and the mixed d_{zx} / d_{zy} / d_{z^2} state at -2.13 eV when this state is shifted to -2.97 eV (Figure 10 vs. Figure 11).

IV. CONCLUSIONS AND INTERPRETATION

The GGA+U structure of Cpd I provides a unique physical perspective on this system, while simultaneously suggesting a manner in which impurity physics may extrapolate to highly magnetic organometallic systems in the large. The behavior observed for $S = 1/2$ and $S = 3/2$ Cpd I models may be justified by considering the assumptions underlying the GGA+U approximation. If the GGA+U energy functional (3) is differentiated with respect to the total orbital occupancy, the resulting value $\epsilon^I_{m\sigma}$ corresponds to the shift in energy eigenvalue for filling a given orbital

$$\epsilon^I_{m\sigma} = \frac{\partial E_U}{\partial n^{I\sigma}_m} = U\left(\frac{1}{2} - n^{I\sigma}_m\right) \tag{10}$$

related to the orbital eigenvalue itself by $\epsilon = \partial E_{\mathrm{GGA+U}}/\partial n^{I\sigma}_m = \epsilon_{\mathrm{GGA}} + \epsilon^I_{m\sigma}$. From this observation, it is apparent that the bare E_{GGA} energy expands by a gap of width $\Delta E = U$ between occupied ($n^I = 1$) and unoccupied ($n^I = 0$) orbital configurations. The effect of this correction mimics the competition between electronic kinetic energy and Coulomb repulsion U within the Hubbard model. If the value of the Hubbard U is large enough, *d*-shell electrons tend to congregate near ionic centers, and correlated behavior emerges due to scattering off of these local moments. The correlated motion inherent in this process then localizes electrons at the impurity site or alternatively leads to complete depletion of electron density at this location. Analogously, the correction E_U to the density functional E_{GGA} ultimately enforces a situation in which increasing values $U \to \infty$ favor unfilled orbitals for fractional orbital occupancies $n^I < 0.5$ and filled orbitals for $n^I \geq 0.5$. In practice, this limit is connected to the uncorrected GGA density functional theory by a continuum of intermediate configurations, each corresponding to a unique value of U.

Since the addition of a Hubbard U term appears to make the DFT description of Cpd I more consistent with experimental expectations, it is possible to lend a sense of physical realism to this inclusion. Reasoning by analogy with results for model Hamiltonians, the perturbed Fe(3*d*) orbitals may be interpreted as impurity states which induce a reorganization of the more weakly correlated DFT electron density on the ligand and porphine subsystems. This redistribution acts to screen the resulting on-site Fe interactions, and likewise

strengthens the nature of spin moments induced by the Fe center. Such a response is particularly apparent for the $S = 1/2$ state, as ascertained by the scaling of magnetization (Figure 3) and spin-density (Figure 4) with increasing U. This behavior is expected of the effective single–particle limit for the full many–body theory, as permitted within the context of DFT. Thus, Cpd I mimics a correlated quantum impurity system in the extremely finite limit.

The aforementioned scenario is far from implausible, as the occupancy and relative energetics of the π^*_{zx}/π^*_{zy} are known to determine not only the excited state structure of Cpd I, but also the distribution of radical character in the system and the ultimately the reactivity of Cpd I.[2] It is precisely this parameter that is tunable through a judicious choice of U. The success of the GGA+U scheme in reproducing a plausible structure for Cpd I is analogous to the success of the hybrid density functionals in reconciling reactivity patterns, branching ratios, and electronic data for this system.[1] More specifically, the GGA approximation suffers from a poor treatment of electron self-interaction for fractionally-occupied orbitals in the exchange correlation component of the density functional. This leads to an unphysical curvature of the energy for such orbital configurations, which may be offset by a judicious choice of U.[42] It is specifically this aberrant exchange correlation that the hybrid functionals themselves were designed to correct, albeit through different means. While the algorithm for determination of U_{SCF}[17] is unable to do this in a physically consistent manner and thus reproduce an energy profile corresponding to the apocryphal "exact density functional," this may have less to do with the logic underlying the algorithm as other hitherto unspecified shortcomings of GGA exchange correlation. More specifically, these discrepancies likely arise through the approximate nature of this particular GGA+U scheme, including the explicit neglect of spin exchange coupling J and the omission of non-spherical interactions by restricting electron-electron scattering processes to channels of equivalent angular momenta.[42] In the presence of these limitations, the self-consistent determination of U is inevitably unsuccessful despite its inherent physical realism. Nonetheless, calculations employing the empirically derived value of U are themselves efficacious, and should in some sense correspond to a "renormalization" of U_{SCF} in the context of these approximations.

Finally, with respect to chemical processes, the distinct GGA+U electronic structure observed in the vicinity of E_F for each ligand and spin state calculation lends support to the so–called multistate reactivity (MSR) hypothesis[2,63] for Cpd I. The MSR posits that the reactivity of Cpd I is dependent on a manifold of factors including spin state, axial ligand environment, and background electric field, with each configuration preferentially catalyzing a different set of chemical transformations. A canonical example is the competition between Cpd I–catalyzed propene hydroxylation and epoxidation, in which the product distribution and even the reaction mechanism itself are dependent on the spin state of Cpd I and the nature of the axial ligand.[64] By extension of this scheme, an enzymatic Cpd I tunes itself, through coupling to the protein environment, to the specific chemistry exploited in a given reaction or stage of a multistep reaction.[65] Exploration of these systems using the GGA+U framework permits an extrapolation to plane–wave based *ab initio* molecular dynamics schemes, while simultaneously affording a physical justification which is obscured by the hybrid density functional framework employed in preceding quantum mechanical and quantum mechanical/molecular mechanical calculations.[1] Specifically extending these DFT+U results to *ab initio* molecular dynamics calculations for the cytochromes P450 would provide an invaluable perspective on molecular oxygen activation, proton transport both into and within the catalytic center, and the electronic structure of reaction intermediates. The calculations reported herein embody a first step in that direction.

ACKNOWLEDGMENTS

The authors are grateful to the Ohio Supercomputer Center and the VCU Center for Life Sciences for a generous allocation of computational resources. This work was supported by a grant from the National Institutes for Health (NIH) (Grant No. GM092827) awarded to J.CH.

[1] S. Shaik, S. Cohen, Y. Wang, H. Chen, D. Kumar, and W. Thiel, Chem. Rev. **110**, 949 (2010).
[2] S. Shaik, D. Kumar, S. P. deVisser, A. Altun, and W. Thiel, Chem. Rev. **105**, 2279–2328 (2005).
[3] T. Higuchi, S. Uzu, and M. Hirobe, J. Am. Chem. Soc. **112**, 7051 (1990).
[4] H. Volz and M. Holzbecher, Angew. Chem., Int. Ed. **36**, 1442 (1997).
[5] H.-A. Wagenknecht and W.-D. Woggon, Angew. Chem., Int. Ed. **36**, 390 (1997).
[6] T. Xue, S. Jiang, Y. Qu, Q. Su, R. Cheng, S. Dubin, C.-Y. Chiu, R. Kaner, Y. Huang, and X. Duan, Angew. Chem., Int. Ed. **51**, 1 (2012).
[7] H. Chen, J. Song, W. Lai, W. Wu, and S. Shaik, J. Chem. Theory Comput. **6**, 940 (2010).
[8] F. Ogliaro, S. Cohen, M. Filatov, N. Harris, and S. Shaik, Angew. Chem., Int. Ed. **39**, 3851 (2000).
[9] C. M. Hosten, A. M. Sullivan, V. Palaniappan, M. M. Fitzgerald, and J. Terner, J. Biol. Chem. **269**, 13966 (1994).
[10] R. Rutter, L. P. Hager, H. Dhonau, M. Hendrich, M. Valentine, and P. Debrunner, Biochemistry **23**, 6809 (1984).
[11] J. Rittle and M. T. Green, Science **330**, 933 (2010).
[12] J. C. Schoneboom, F. Neese, and W. Thiel, J. Am. Chem. Soc. **127**, 5840 (2005).
[13] J. Hubbard, Proc. R. Soc. London, Ser. A **276**, 238 (1963).
[14] E. Fradkin, *Field Theories of Condensed Matter Systems* (Westview, 1998).
[15] V. I. Anisimov, J. Zaanen, and O. K. Andersen, Phys. Rev. B **44**, 943 (1991).
[16] V. I. Anisimov, F. Aryasetiawan, and A. I. Lichtenstein, J. Phys.: Condens. Matter **9**, 767 (1997).
[17] H. J. Kullik, M. Cococcioni, D. A. Scherlis, and N. Marzari, Phys. Rev. Lett. **97**, 103001 (2006).
[18] D. A. Scherlis, M. Cococcioni, P. Sit, and N. Marzari, J. Phys. Chem. B **111**, 7384 (2007).
[19] H. J. Kulik and N. Marzari, J. Chem. Phys. **129**, 134314 (2008).
[20] P. M. Panchmatia, B. Sanyal, and P. M. Oppeneer, Chem. Phys. **343**, 47 (2008).
[21] P. M. Panchmatia, M. E. Ali, B. Sanyal, and P. M. Oppeneer, J. Phys. Chem. A **114**, 13381 (2010).
[22] M. E. Ali, B. Sanyal, and P. M. Oppeneer, J. Phys. Chem. B **116**, 5849 (2012).
[23] R. Car and M. Parrinello, Phys. Rev. Lett. **55**, 2471 (1986).
[24] D. Marx and M. Parrinello, Z. Phys. B: Condens. Matter **95**, 143 (1994).
[25] D. Marx and M. Parrinello, J. Chem. Phys. **104**, 4077 (1996).
[26] C. Rovira, Chem. Phys. Chem. **6**, 1820 (2005).
[27] P. Vidossich, M. Alfonso-Prieto, X. Carpena, P. C. Loewen, I. Fita, and C. Rovira, J. Am. Chem. Soc. **129**, 13436 (2007).
[28] M. Alfonso-Prieto, A. Borovik, X. Carpena, G. Murshudov, W. Melik-Adamyan, I. Fita, C. Rovira, and P. C. Loewen, J. Am. Chem. Soc. **129**, 4193 (2007).

[29]M. Alfonso-Prieto, P. Vidossich, A. Rodriguez-Fortea, X. Carpena, I. Fita, P. C. Loewen, and C. Rovira, J. Phys. Chem. A **112**, 12842 (2008).
[30]M. Alfonso-Prieto, X. Biarnes, P. Vidossich, and C. Rovira, J. Am. Chem. Soc. **131**, 11751 (2009).
[31]P. Vidossich, X. Carpena, P. C. Loewen, I. Fita, and C. Rovira, J. Phys. Chem. Lett. **2**, 196 (2011).
[32]C. Rovira, P. Ballone, and M. Parrinello, Chem. Phys. Lett. **271**, 247 (1997).
[33]C. Rovira, K. Kunc, J. Hutter, P. Ballone, and M. Parrinello, J. Phys. Chem. A **101**, 8914 (1997).
[34]C. Rovira, K. Kunc, J. Hutter, P. Ballone, and M. Parrinello, Int. J. Quantum Chem. **69**, 31 (1998).
[35]L. G. D. da Silva, M. L. Tiago, S. E. Ulloa, F. A. Reboredo, and E. Dagotto, Phys. Rev. B **80**, 155443 (2009).
[36]A. M. P. Sena, V. Brazdova, and D. R. Bowler, Phys. Rev. B **79**, 245404 (2009).
[37]V. I. Anisimov, I. V. Solovyev, M. A. Korotin, M. T. Czyzyk, and G. A. Sawatzky, Phys. Rev. B **48**, 16929 (1993).
[38]I. V. Solovyev, P. H. Dederichs, and V. I. Anisimov, Phys. Rev. B **50**, 16861 (1994).
[39]A. I. Lichtenstein, M. I. Katsnelson, and G. Kotliar, Phys. Rev. Lett. **87**, 067205 (2001).
[40]A. I. Lichtenstein, V. I. Anisimov, and J. Zaanen, Phys. Rev. B **52**, R5467 (1995).
[41]S. L. Dudarev, G. A. Botton, S. Y. Savrasov, C. J. Humphreys, and A. P. Sutton, Phys. Rev. B **57**, 1505 (1998).
[42]M. Cococcioni and S. de Gironcoli, Phys. Rev. B **71**, 035105 (2005).
[43]V. I. Anisimov and O. Gunnarsson, Phys. Rev. B **43**, 7570–7574 (1991).
[44]P. Giannozzi, S. Baroni, N. Bonini, M. Calandra, R. Car, C. Cavazzoni, D. Ceresoli, G. L. Chiarotti, M. Cococcioni, I. Dabo, A. D. Corso, S. de Gironcoli, S. Fabris, G. Fratesi, R. Gebauer, U. Gerstmann, C. Gougoussis, A. Kokalj, M. Lazzeri, L. Martin-Samos, N. Marzari, F. Mauri, R. Mazzarello, S. Apolini, A. Pasquarello, L. Paulatto, C. Sbraccia, S. Scandolo, G. Sclauzero, A. P. Seitsonen, A. Smogunov, P. Umari, and R. M. Wentzcovitch, J. Phys: Condens. Matter **21**, 395502 (2009).
[45]J. P. Perdew, K. Burke, and M. Ernzerhof, Phys. Rev. Lett. **77**, 3865 (1996).
[46]D. Vanderbilt, Phys. Rev. B **41**, 7892 (1990).
[47]F. Neese, ORCA — an *ab initio* density functional, and semiempirical program package, version 2.7, University of Bonn (2008).
[48]F. Wiegend and R. Ahlrichs, Phys. Chem. Chem. Phys. **7**, 3297 (2005).
[49]C. Adamo and V. Barone, J. Chem. Phys. **110**, 6158 (1999).
[50]R. Ahlrichs, M. Bar, M. Haser, H. Horn, and C. Kolmel, Chem. Phys. Lett. **162**, 165 (1989).
[51]G. Henkelman, A. Arnaldsson, and H. Jonsson, Comput. Mater. Sci. **36**, 254 (2006).
[52]E. Sanville, S. D. Kenney, R. Smith, and G. Henkelman, J. Comput. Chem. **28**, 899 (2007).
[53]W. Tang, E. Sanville, and G. Henkelman, J. Phys: Condens. Matter **21**, 084204 (2009).
[54]H. Wende, M. Bernien, J. Luo, C. Sorg, N. Ponpandian, J. Kurde, J. Miguel, M. Piantek, X. Xu, P. Eckhold, W. Kuch, K. Baberschke, P. M. Panchmatia, B. Sanyal, P. M. Oppeneer, and O. Eriksson, Nature Mater. **6**, 516 (2007).
[55]P. M. Oppeneer, P. M. Panchmatia, B. Sanyal, O. Eriksson, and M. E. Ali, Prog. Surf. Sci. **84**, 18 (2009).
[56]K. L. Stone, R. K. Behan, and M. T. Green, Proc. Natl. Acad. Sci. U.S.A. **102**, 16563 (2005).
[57]P. Gans, G. Buisson, E. Duee, J.-C. Marchon, B. S. Erler, W. F. Scholz, and C. A. Reed, J. Am. Chem. Soc. **108**, 1223 (1986).
[58]S. H. Kim, R. Perera, L. P. Hager, J. H. Dawson, and B. M. Hoffman, J. Am. Chem. Soc. **128**, 5598 (2006).
[59]H. Hirao, D. Kumar, W. Thiel, and S. Shaik, J. Am. Chem. Soc. **127**, 13007 (2005).
[60]A. Altun, S. Shaik, and W. Thiel, J. Am. Chem. Soc. **129**, 8978 (2007).
[61]H. J. Kulik and N. Marzari, J. Chem. Phys. **133**, 114103 (2010).
[62]See supplementary material at http://dx.doi.org/10.1063/1.4755290 for Hubbard U scaling of thiolate ligated models, molecular geometries and spin density distributions.
[63]S. Shaik, S. P. deVisser, F. Ogliaro, H. Schwarz, and D. Schroder, Curr. Opin. Chem. Biol. **6**, 556 (2002).
[64]S. P. deVisser, F. Ogliaro, P. K. Sharma, and S. Shaik, J. Am. Chem. Soc. **124**, 11809 (2002).
[65]F. Ogliaro, S. Cohen, S. P. deVisser, and S. Shaik, J. Am. Chem. Soc. **122**, 12892 (2000).